DDA3 recruits microtubule depolymerase Kif2a to spindle poles and controls spindle dynamics and mitotic chromosome movement

Chang-Young Jang,[1] Jim Wong,[1] Judith A. Coppinger,[2] Akiko Seki,[1] John R. Yates III,[2] and Guowei Fang[1]

[1]Department of Biological Sciences, Stanford University, Stanford, CA 94305
[2]Department of Chemical Physiology, The Scripps Research Institute, La Jolla, CA 92037

Dynamic turnover of the spindle is a driving force for chromosome congression and segregation in mitosis. Through a functional genomic analysis, we identify DDA3 as a previously unknown regulator of spindle dynamics that is essential for mitotic progression. DDA3 depletion results in a high frequency of unaligned chromosomes, a substantial reduction in tension across sister kinetochores at metaphase, and a decrease in the velocity of chromosome segregation at anaphase. DDA3 associates with the mitotic spindle and controls microtubule (MT) dynamics. Mechanistically, DDA3 interacts with the MT depolymerase Kif2a in an MT-dependent manner and recruits Kif2a to the mitotic spindle and spindle poles. Depletion of DDA3 increases the steady-state levels of spindle MTs by reducing the turnover rate of the mitotic spindle and by increasing the rate of MT polymerization, which phenocopies the effects of partial knockdown of Kif2a. Thus, DDA3 represents a new class of MT-destabilizing protein that controls spindle dynamics and mitotic progression by regulating MT depolymerases.

Introduction

The mitotic spindle controls chromosome congression and segregation through dynamic polymerization and depolymerization of microtubules (MTs; Gadde and Heald, 2004). Active turnover of MTs allows the mitotic spindle to efficiently probe the three-dimensional cytoplasmic space for bipolar attachment of sister kinetochores and to congress chromosomes to the metaphase plate. MT dynamics also generates a pulling force, or tension, across sister kinetochores that is monitored by the spindle checkpoint (Musacchio and Hardwick, 2002). The presence of a single unattached kinetochore or under-tensed sister kinetochores activates the checkpoint and delays anaphase onset to prevent unequal segregation of chromosomes. Unattached and under-tensed kinetochores actively recruit checkpoint proteins, such as Mad2 and BubR1, to kinetochores, leading to the inhibition of the anaphase-promoting complex/cyclosome and a mitotic arrest (Musacchio and Salmon, 2007). Once all the kinetochores are attached and under tension, the checkpoint is turned off and MT depolymerization provides a driving force for chromosome segregation at anaphase.

MTs are dynamically unstable and switch between growing and shrinking phases (Desai and Mitchison, 1997; Kline-Smith and Walczak, 2004). Spindle dynamics is regulated by MT nucleators such as γ-tubulin, by MT depolymerases such as the kinesin-13 family of proteins, and by MT-associated proteins (MAPs). MAPs can be categorized into MT-stabilizing factors, such as TPX2, HURP, and ch-TOG, and destabilizing factors, such as katanin and Op18/stathmin (Gadde and Heald, 2004; Kline-Smith and Walczak, 2004; Maiato et al., 2004). Many MT-stabilizing proteins have been characterized mechanistically: they directly bind to and enhance the MT stability in general. In contrast, limited information is available on MT-destabilizing proteins. The two best-characterized destabilizing MAPs are katanin and Op18. Katanin destabilizes the mitotic spindle by severing MTs and Op18 sequesters the α/β-tubulin dimers and stimulates catastrophes (Kline-Smith and Walczak, 2004). The kinesin-13 family of MT depolymerases has three members, Kif2a, Kif2b, and MCAK/Kif2c, each with diverse functions in mitosis (Wordeman, 2005). Kif2a directly binds to MT ends in vitro (Desai et al., 1999) and is localized to spindle poles in vivo to control bipolar spindle assembly (Ganem and Compton, 2004). MCAK/Kif2c is localized to inner centromeres and to spindle MTs and is essential for correct attachment of MTs to kinetochores (Kline-Smith and Walczak, 2004; Wordeman, 2005). Finally, Kif2b is localized to the centrosomes and plays roles in bipolar spindle assembly, chromosome movement, and cytokinesis (Manning et al., 2007).

Correspondence to Guowei Fang: gwfang@stanford.edu

Abbreviations used in this paper: FLIP, fluorescence loss in photobleaching; MAP, MT-associated protein; MT, microtubule.

The Journal of Cell Biology, Vol. 181, No. 2, April 21, 2008 255–267
http://www.jcb.org/cgi/doi/10.1083/jcb.200711032

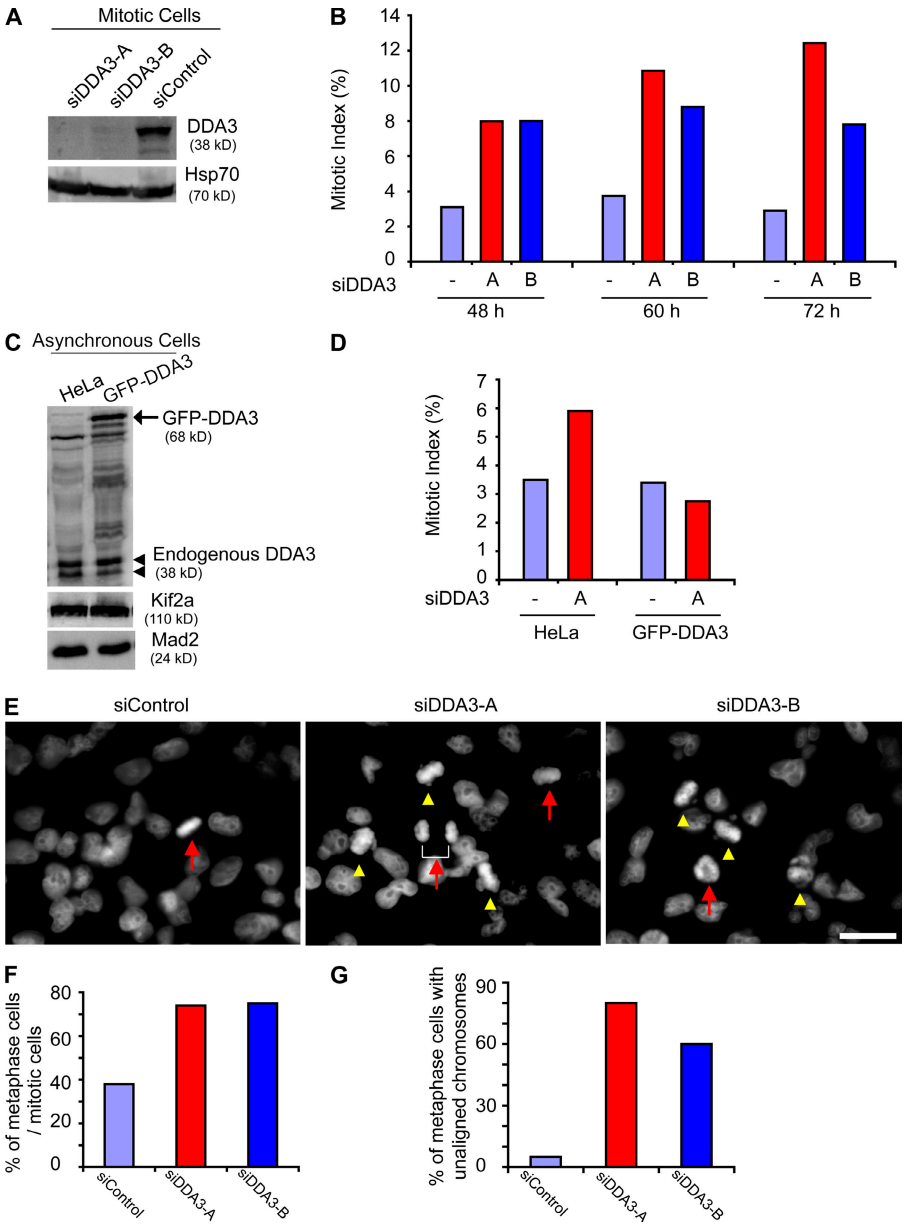

Figure 1. **DDA3 controls mitotic progression.** (A) HeLa cells were transfected with control (siControl) or DDA3-specific siRNAs (siDDA3-A and -B), synchronized at prometaphase by a thymidine-nocodazole treatment, and analyzed by Western blotting. Hsp70 served as a loading control. (B) HeLa cells were transfected with siRNAs and collected at the indicated times after transfection. Mitotic index was determined by FACS with anti-MPM2 antibody staining. The MPM2 antibody recognizes mitotic phosphoproteins and was used to determine mitotic index. (C) HeLa cells or HeLa cells stably expressing GFP–DDA3 (HeLa/GFP–DDA3) were analyzed by Western blotting to determine the levels of GFP–DDA3 relative to the endogenous DDA3. Mad2 served as a loading control. Arrowheads point to endogenous DDA3. Bands above endogenous DDA3 in the HeLa lane represent cross reacting proteins. (D) HeLa or HeLa/GFP–DDA3 cells were transfected with siControl or siDDA3-A and collected at 56 h after transfection. Mitotic index was determined by FACS analysis. (E–G) HeLa cells were transfected with siRNAs and stained for DNA (E) at 62 h after transfection. Arrows point to normal mitotic cells. Arrowheads point to metaphase cells with unaligned chromosomes. The percentage of metaphase cells over total mitotic cells (F) and the percentage of metaphase cells with unaligned chromosomes over total metaphase cells (G) were quantified and plotted. Bar, 20 μm.

To identify novel regulators of spindle dynamics and chromosome movement, we undertook a genomic analysis to identify candidate mitotic genes based on their expression profiles (Wong and Fang, 2006; Zhao et al., 2006; Seki and Fang, 2007). Subsequent functional analysis of these genes in a targeted siRNA screen identified DDA3 as a regulator of the mitotic spindle. DDA3 was initially discovered by differential display as a target of the tumor suppressor p53 but its physiological function remains unknown (Lo et al., 1999). In this paper, we describe DDA3 as a MAP that functions on the mitotic spindle. Metaphase cells depleted of DDA3 had a high frequency of unaligned chromosomes and a substantial reduction in interkinetochore tension for aligned chromosomes, resulting in activation of the spindle checkpoint and a mitotic arrest. DDA3 destabilized the mitotic spindle, reduced the kinetics of MT polymerization, and increased the spindle turnover rate. Biochemically, DDA3 directly interacted with the MT depolymerase Kif2a in an MT-dependent manner and increased the efficiency of targeting Kif2a to spindle poles. We conclude that DDA3 regulates the localization of an MT depolymerase and controls MT dynamics and chromosome movement.

Results

DDA3 controls mitotic progression

We have previously developed a systems approach to efficiently identify candidate mitotic regulators based on their transcription pattern (Wong and Fang, 2006; Zhao et al., 2006; Seki and Fang, 2007). Our analyses were based on the following two observations. First, expression of cell cycle regulators covaries (coupregulates or corepresses) during tumorigenesis, as selective pressure for tumor proliferation constrains cell cycle regulators for coordinated expression (Segal et al., 2004). Second, genes induced in G2 or M are likely to function in mitosis. Thus, we searched published microarray databases for novel G2/M-induced genes

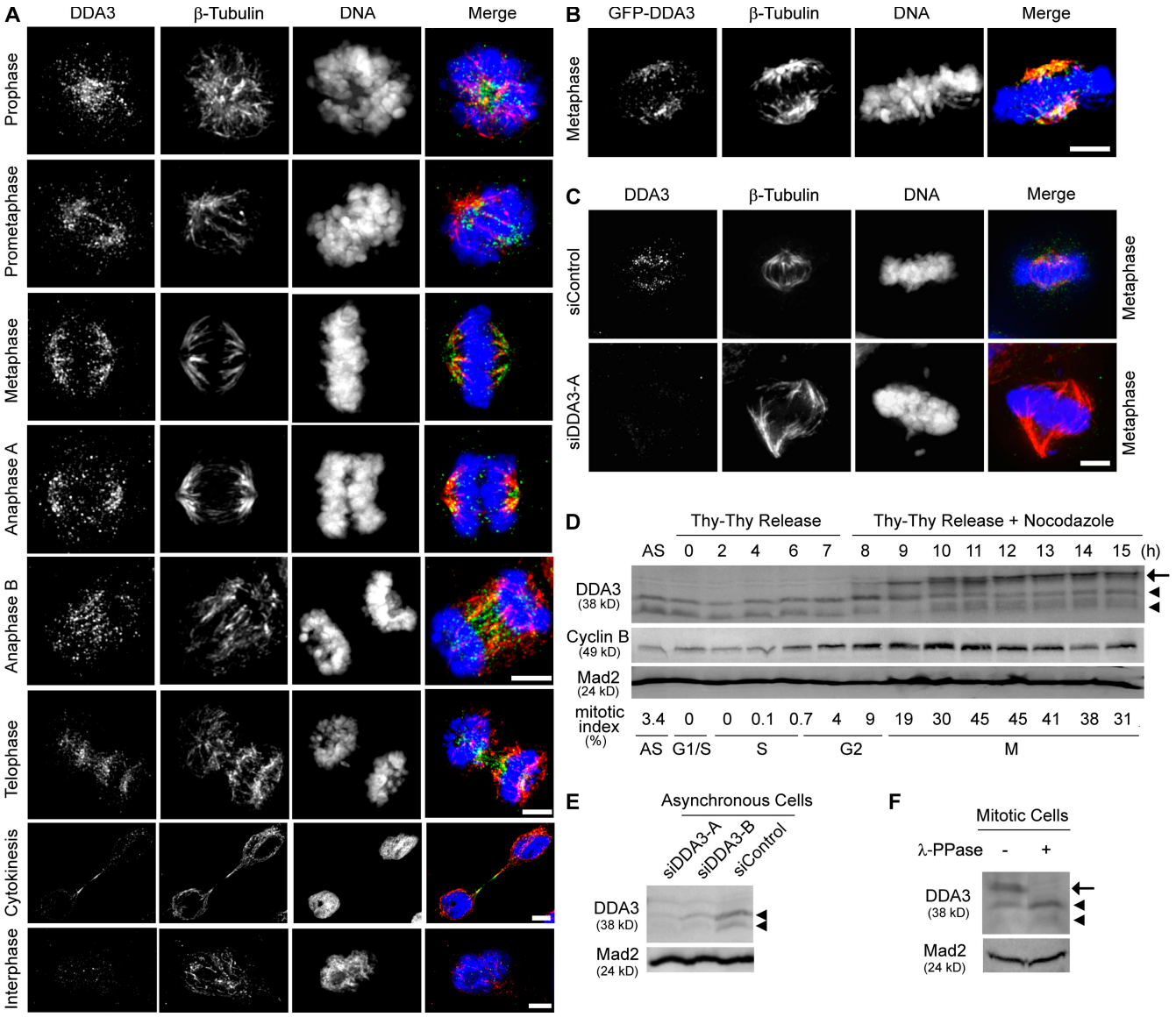

Figure 2. **DDA3 is a spindle-associated cell cycle protein.** (A–C) Shown are maximum projections from deconvolved z stacks of representative cells stained for DDA3 (A and C, green)/GFP (B, green), β-tubulin (red), and DNA (blue). A, HeLa cells; B, HeLa/GFP–DDA3 cells; C, HeLa cells transfected with siControl or siDDA3-A. Bars, 5 μm. (D) HeLa cells were synchronized by a double-thymidine treatment and released into fresh media. 150 ng/ml nocodazole was added at 8 h after release and cells were harvested at the indicated times. Cells were analyzed by FACS and Western blotting. AS, unsynchronized cells. (E) HeLa cells were transfected with siRNAs, harvested at 62 h as asynchronous cells, and analyzed to identify DDA3-specific bands on Western blot. (F) Lysates of thymidine-nocodazole–treated mitotic HeLa cells were incubated with or without λ-phosphatase (λ-PPase) before immunoblotting to identify phosphorylated DDA3. Arrows point to hyperphosphorylated mitotic DDA3 and arrowheads point to two forms of hypo- or unphosphorylated DDA3.

(Whitfield et al., 2002) whose expression covaries with that of known cell cycle regulators across hundreds of tumor tissues (Segal et al., 2004). The function of these candidate genes was analyzed in a targeted siRNA screen for an increase in mitotic index as an indication of defects in mitosis in knockdown cells.

One gene identified was DDA3, whose knockdown resulted in a two- to fourfold increase in mitotic index as measured by FACS (Fig. 1, A and B). This phenotype is specific, as a similar increase in mitotic index was generated by two independent siRNAs (siDDA3-A and siDDA3-B), both of which efficiently knocked down endogenous DDA3 by >90% (Fig. 1, A and B). To further confirm the knockdown phenotype, we generated a HeLa cell line stably expressing GFP fused to the coding sequence of DDA3 at a level approximate to that of the endogenous DDA3 (Fig. 1 C). As expected, expression of GFP–DDA3 rescued the high mitotic index phenotype generated by a siRNA (siDDA3-A) targeting to the 3′ noncoding sequence of the endogenous DDA3 gene (Fig. 1 D).

Further analysis revealed a twofold increase in metaphase-like cells among DDA3-depleted mitotic cells when compared with control samples (Fig. 1, E and F). Among metaphase cells, there is a >10-fold increase in cells with unaligned chromosomes upon depletion of DDA3 (80, 60, and 5% in siDDA3-A, siDDA3-B, and control cells, respectively; Fig. 1, E and G). We conclude that DDA3 is a novel cell cycle regulator that is essential for chromosome congression and mitotic progression.

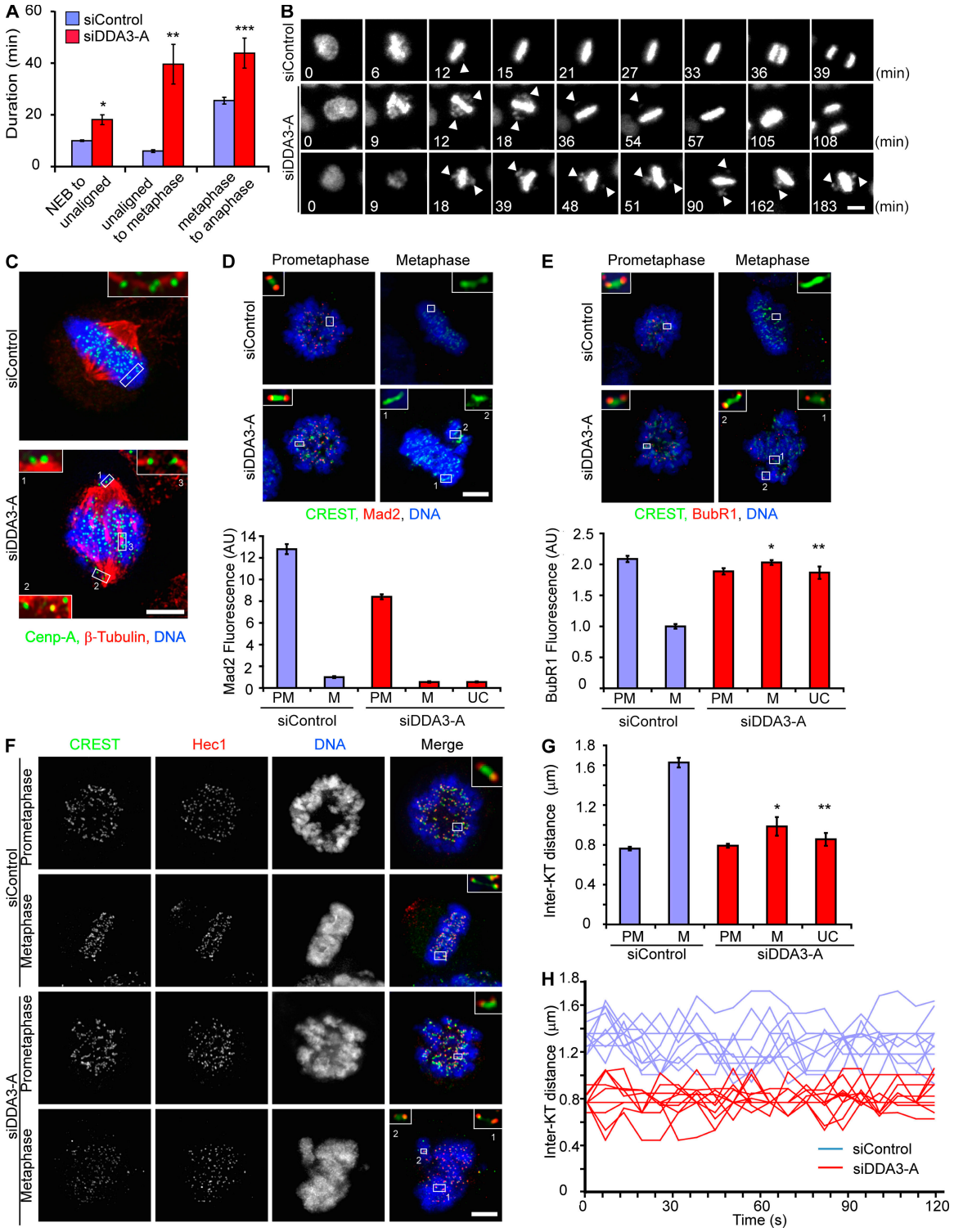

Figure 3. **Depletion of DDA3 prolongs metaphase and activates the spindle checkpoint.** (A and B) HeLa/GFP-Histone H2B cells were transfected with siRNAs and imaged for GFP-Histone H2B by time lapse starting from 50 h after transfection. Images were captured every 3 min to monitor mitotic progression. The duration from nuclear envelop breakdown (NEB) to the formation of a bipolar spindle/metaphase plate with some unaligned chromosomes (NEB to unaligned), from the unaligned state to metaphase without unaligned chromosomes (unaligned to metaphase), and from metaphase without unaligned chromosomes to anaphase (metaphase to anaphase) were determined for control and DDA3-depleted cells (n = 30 cells). Still frames from time-lapse movies of representative cells are shown in B. Arrowheads point to unaligned chromosomes. *, $P < 0.0013$; **, $P < 6 \times 10^{-5}$; ***, $P < 0.0026$ (two-tailed t test). (C) HeLa cells were transfected with siRNAs. At 50 h after transfection, cells were incubated at 4°C for 10 min, fixed, and stained for kinetochore MTs. Shown are maximum projections from deconvolved z stacks of representative cells stained for CenpA (green), β-tubulin (red), and DNA (blue). Insets show single focal planes of boxed regions. (D and E) Shown are maximum projections from deconvolved z stacks of representative control or DDA3-depleted HeLa cells stained for CREST (green), Mad2 (D, red)/ BubR1 (E, red), and DNA (blue). Insets show single focal planes of boxed regions. Mad2 and BubR1 signals on kinetochores were quantified in five control or DDA3-depleted cells at prometaphase (PM) or metaphase (M; $n > 100$ kinetochores for each quantification). For unaligned chromosomes (UC) in DDA3-depleted metaphase cells, 40 kinetochores on unaligned chromosomes from 10 metaphase cells

DDA3 is a spindle-associated cell cycle protein

To elucidate its role in mitosis, we determined the cellular localization of endogenous DDA3 across the cell cycle. DDA3 punctately colocalized with spindle MTs from prophase to anaphase A and with the central spindle and midbody MTs from anaphase B to the end of cytokinesis (Fig. 2 A). DDA3 was diffusively distributed throughout the cell without obvious localization to MTs in interphase cells, indicating that the association of DDA3 with the mitotic spindle is under active regulation. This cell cycle–dependent localization of DDA3 is specific, as stably expressed GFP–DDA3 also localized to the mitotic spindle (Fig. 2 B; Hsieh et al., 2007) and as knockdown of DDA3 completely abolished its localization on the spindle (Fig. 2 C).

Next, we examined the levels of the DDA3 protein across the cell cycle. HeLa cells were arrested at the G1/S boundary by a double-thymidine (Thy–Thy) treatment and then released into fresh media for synchronous cell cycle progression (Fang et al., 1998a,b). 8 h after release, cells were treated with nocodazole to accumulate mitotic cells. The cell cycle profile was analyzed by FACS and the protein levels were analyzed by Western blotting (Fig. 2 D). The levels of DDA3 were relatively low in asynchronous cells and in G1/S cells but slowly increased in late G2 and mitosis. This pattern of expression is similar to but less dramatic than that of cyclin B across the cell cycle.

We noticed the existence of multiple forms of DDA3 across the cell cycle (Fig. 2 D). In asynchronous cells and in G1/S cells, DDA3 existed as a doublet, both of which were depleted by siRNAs targeted to DDA3 (Fig. 2 E). The nature of this doublet remains to be determined, but it may represent alternatively spliced forms of DDA3. Mitotic DDA3 was upshifted and this shifted band was efficiently knockdown by siDDA3 (Fig. 1 A), confirming the specificity of the Western signal. The shifted DDA3 corresponds to the phosphorylated protein, as this mobility change was abolished by the λ-phosphatase treatment (Fig. 2 F). Thus, DDA3 is a cell cycle–regulated phosphoprotein localized to the mitotic spindle.

Depletion of DDA3 delays mitotic progression and activates the spindle checkpoint

The cellular function of DDA3 was analyzed by time-lapse imaging of HeLa cells stably expressing GFP-Histone H2B (Fig. 3, A and B). Quantitative analysis of mitotic progression indicated that depletion of DDA3 altered the duration of prometaphase (from nuclear envelope breakdown to initial formation of the metaphase plate) to some extent but more significantly prolonged the duration of metaphase (from the initial formation of the metaphase plate to anaphase onset; Fig. 3 A). This extended metaphase mainly resulted from the persistence of unaligned chromosomes in metaphase cells depleted of DDA3 (Fig. 3 A, unaligned to metaphase). However, this is only a kinetic delay at metaphase. The majority of unaligned chromosomes eventually congressed to the metaphase plate (Fig. 3, A and B), followed by anaphase initiation, even though a certain percentage (20 and 1% for siDDA3-A and siControl metaphase cells, respectively) of transfected cells with a large number of unaligned chromosomes underwent apoptosis after extended arrest at metaphase. Thus, DDA3 is required for efficient chromosome congression to the metaphase plate and for timely onset of anaphase.

To determine whether the lack of congression of unaligned chromosomes resulted from an absence of MT attachment, we directly analyzed the MT–kinetochore interactions in cold-treated HeLa cells depleted of DDA3 and found that the majority of kinetochores on unaligned chromosomes in metaphase cells were attached to MTs (Fig. 3 C). To gain a statistically representative conclusion, we analyzed the fluorescence intensity of the kinetochore-associated checkpoint protein Mad2, which monitors the MT occupancy on kinetochores (Skoufias et al., 2001; Musacchio and Salmon, 2007). Mad2 was present on kinetochores of both control and DDA3 knockdown cells at prometaphase. However, this checkpoint protein disappeared from kinetochores in metaphase cells, including those on the unaligned chromosomes in knockdown cells (Fig. 3 D). Thus, MTs are attached to kinetochores of unaligned chromosomes. We next analyzed whether the MT attachment generated tension across sister kinetochores, which is monitored by the kinetochore-associated checkpoint protein BubR1 (Skoufias et al., 2001; Musacchio and Salmon, 2007). In control cells, tension is established in metaphase cells but not in prometaphase cells. As expected, the BubR1 fluorescence intensity on kinetochore was higher in control prometaphase cells than in control metaphase cells (Fig. 3 E). However, knockdown of DDA3 abolished the tension across sister kinetochores in metaphase cells, and a large number of chromosomes aligned at the metaphase plate retained high levels of BubR1 signals on kinetochores (Fig. 3 E).

Interkinetochore tension is generated by the pulling force derived from dynamic turnover of attached MTs. The presence of the pulling force increased the interkinetochore distance in control cells from prometaphase (0.77 ± 0.02 μm) to metaphase (1.63 ± 0.05 μm; Fig. 3, F and G). However, the interkinetochore distance of chromosomes aligned at the metaphase plate in DDA3-depleted cells (0.99 ± 0.09 μm) was substantially shorter than that in control metaphase cells, again indicating a

were quantified. *, $P < 6 \times 10^{-32}$; **, $P < 6 \times 10^{-10}$ (two-tailed *t* test relative to siControl metaphase cells). AU, arbitrary units. (F and G) Shown are maximum projections from deconvolved z stacks of representative control or DDA3-depleted HeLa cells stained for CREST (green), Hec1 (red), and DNA (blue). Images were collected with a 100× objective lens without binning. Interkinetochore (Inter-KT) distance in prometaphase and metaphase cells was quantified from >100 kinetochore pairs in five cells for each quantification. For unaligned chromosomes in DDA3-depleted metaphase cells, 10 kinetochore pairs were quantified. Boxes 1 and 2 in D–F represent aligned and unaligned chromosomes in DDA3-depleted metaphase cells, respectively. *, $P < 5 \times 10^{-57}$; **, $P < 1.1^{-4}$ (two-tailed *t* test relative to siControl metaphase cells). (H) HeLa cells stably expressing GFP-CenpA were transfected with siRNAs and imaged for GFP-CenpA by time lapse. Images were acquired every 6 s on a spinning disc confocal microscope using a 63× objective lens with 2 × 2 binning. Interkinetochore distance of individual kinetochore pairs from chromosomes aligned at the metaphase plate was tracked and plotted over 60 s. Error bars show SEM. Bars: (B) 10 μm; (C–F) 5 μm.

lack of tension. This conclusion was independently confirmed by directly measuring the interkinetochore distance through time-lapse imaging of GFP-CenpA cells (Fig. 3 H). Thus, depletion of DDA3 abolished tension across sister kinetochores, leading to activation of the spindle checkpoint.

DDA3 controls the dynamics of the mitotic spindle

To understand how spindle-associated DDA3 controls chromosome congression and interkinetochore tension, we investigated the role of DDA3 in spindle assembly, dynamics, and function. First, the interpolar distance, as marked by pericentrin signals, was longer in DDA3-depleted cells (13.68 ± 0.6 μm) than in control cells (9.02 ± 0.23 μm; Fig. 4, A and B). Thus, spindle morphology was altered in DDA3 knockdown cells. Second, MT density, as measured by total β-tubulin immunofluorescence intensity, was increased by 50% in DDA3-depleted cells compared with control cells (Fig. 4 C). Under conditions that destabilize MTs, such as cold or limited incubation with nocodazole, MT density was also higher in DDA3 knockdown cells than in control cells (Fig. 4 C). Thus, DDA3 destabilizes the spindle MTs in mitosis. Consistent with this conclusion, MTs in a GFP–DDA3 stable cell line (Fig. 1 C) were more sensitive to the treatment by nocodazole and cold than those in control cells, even though the total amounts of MTs in untreated GFP–DDA3 cells were slightly higher than those in untreated parental cells (Fig. 4 D).

To investigate the role of DDA3 on spindle dynamics, we determined the kinetics of MT polymerization. Cells were transfected with siControl or siDDA3-A and treated with 1 μg/ml nocodazole to completely depolymerize MTs. Cells were then released into fresh media and the rate of MT polymerization was analyzed kinetically. DDA3-depleted mitotic cells repolymerized MTs faster than control cells (Fig. 4, E and F). Depletion of DDA3 by siDDA3-B gave a similar phenotype, confirming its specificity (Fig. 4 G). Thus, DDA3 destabilizes the mitotic spindle and inhibits MT growth. This conclusion is also supported by stable expression of GFP–DDA3, which reduced the rate of MT repolymerization after nocodazole treatment (Fig. 4 H).

Effect of DDA3 on spindle dynamics was directly analyzed in a fluorescence loss in photobleaching (FLIP) experiment that measures the turnover rate of α/β-tubulin heterodimers on the mitotic spindle. HeLa cells stably expressing GFP–α-tubulin were transfected with a control or siDDA3, and the cytoplasm of metaphase cells was photobleached continuously while time-lapse images were captured every 0.58 s to record the decrease in GFP fluorescence on the spindle (Fig. 4 I). The half-life of GFP–α-tubulin on the control metaphase spindle was 170 ± 13 s. This was increased to 361 ± 62 s in siDDA3 metaphase spindles. Thus, DDA3 increases the rate of MT turnover on metaphase spindles, which contributes to the generation of tension across sister kinetochores.

As anaphase chromosome segregation requires dynamic turnover of MTs (Grishchuk and McIntosh, 2006), we predicted that depletion of DDA3 would affect anaphase chromosome movement. Indeed, knockdown of DDA3 reduced the rate of chromosome segregation by >30% in anaphase cells (Fig. 4 J), which is consistent with its role in destabilization of MTs.

DDA3 recruits the MT depolymerase Kif2a to the mitotic spindle and spindle poles

We next identified the cellular target of DDA3 that is responsible for regulating spindle dynamics. The amounts and dynamics of spindle MTs are controlled by MT nucleation/polymerization mediated by the γ-tubulin complex and by MT depolymerization mediated by depolymerases (Kline-Smith and Walczak, 2004; Wordeman, 2005). Our analysis indicated that knockdown of DDA3 did not affect the localization and fluorescence intensity of γ-tubulin (not depicted) but substantially reduced the amounts of depolymerase Kif2a associated with the mitotic spindle and spindle poles (Fig. 5, A and C). DDA3 specifically controls the localization of Kif2a but not the intracellular levels of the Kif2a protein (Fig. 5 D). Furthermore, this effect was specific to Kif2a, but not to other MT depolymerases, such as Kif2c/MCAK and Kif18a (Fig. 5 C and not depicted). Similarly, DDA3 did not control the localization of other proteins associated with spindle poles, such as Aurora A and NuMA, or of general MAPs, such as HURP and TPX2 (Fig. 5, B and C; and not depicted).

A functional connection between DDA3 and Kif2a was confirmed in GFP–DDA3 cells. The levels of DDA3 in GFP–DDA3 cells (endogenous DDA3 plus GFP–DDA3) were approximately doubled compared with the parental cells, whereas the levels of Kif2a were not altered (Fig. 1 C and see Fig. 7 D). Interestingly, the amounts of spindle and spindle pole–associated Kif2a in GFP–DDA3 cells were higher than those in GFP cells (Fig. 5, E and F). Thus, DDA3 recruits Kif2a to the mitotic spindle and spindle poles and controls spindle dynamics.

Partial knockdown of Kif2a phenocopies the depletion of DDA3

To directly determine the effect of Kif2a on spindle dynamics, we analyzed the spindle morphology and dynamics in Kif2a knockdown cells. To mimic the effect of DDA3 depletion on the Kif2a localization, we only partially knocked down Kif2a (~30% Kif2a remained in knockdown cells; Fig. 6 A). Under this condition, the bipolar spindle formed and the Kif2a signals were reduced, but not abolished, from spindle poles (unpublished data). Partial knockdown of Kif2a increased mitotic index and accumulated metaphase cells with unaligned chromosomes (Fig. 6, B and C). Time-lapse analysis indicated a delay in mitotic progression at early metaphase because of the presence of unaligned chromosomes (Fig. 6, D and E), although this delay was transient and less severe than that observed in DDA3 knockdown cells (Fig. 3, A and B).

Kif2a controls the spindle structure, as partial depletion of Kif2a increased the pole-to-pole distance and the amounts of MTs in the bipolar spindle in metaphase cells (Fig. 6, F and G). In the MT repolymerization assay, partial knockdown of Kif2a promoted MT polymerization upon release from nocodazole treatment (Fig. 6 H). Like DDA3, Kif2a regulates spindle dynamics. In the FLIP experiments, knockdown of Kif2a increased the half-lives of mitotic spindles from 170 ± 13 s in control cells

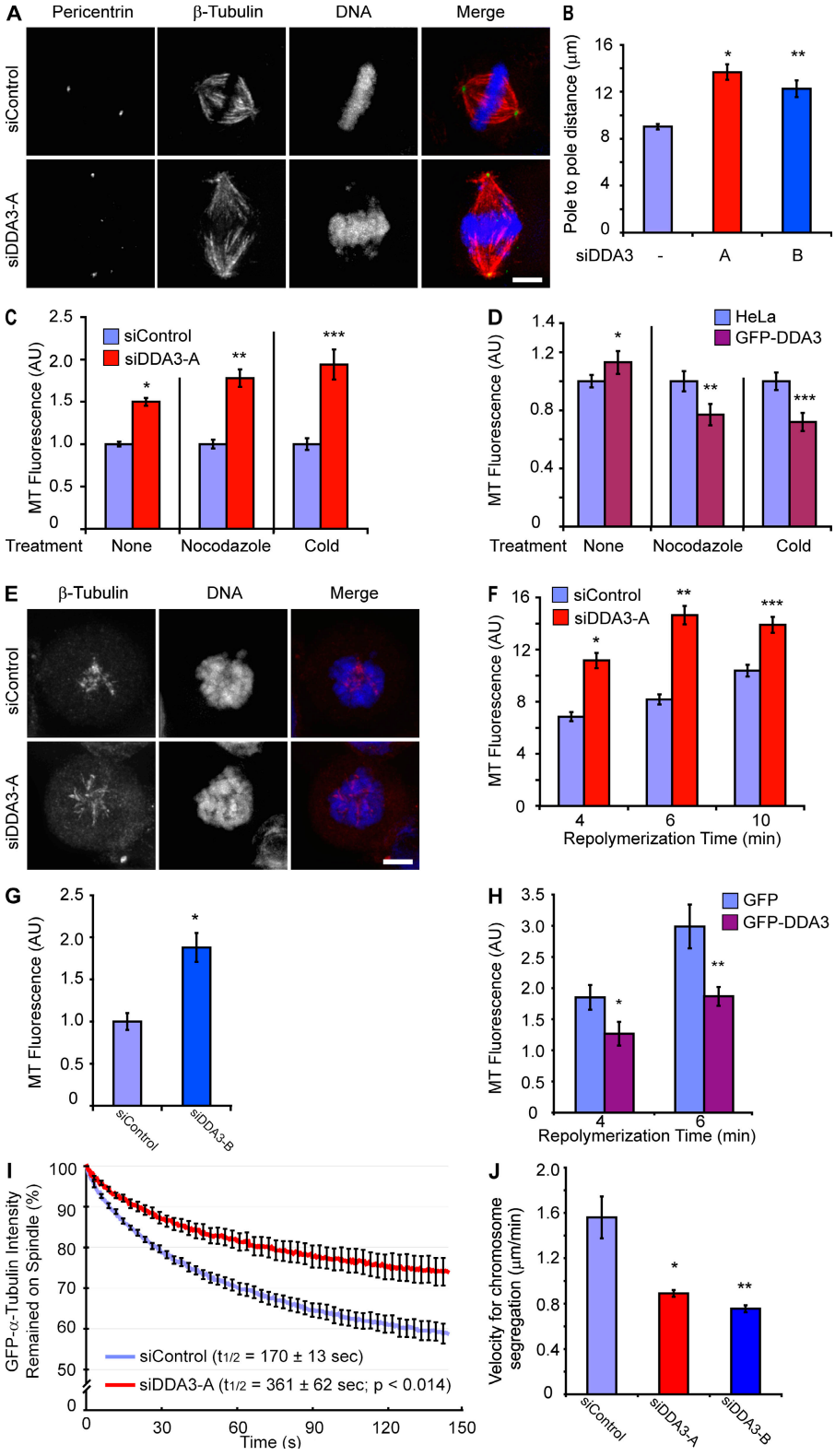

Figure 4. **DDA3 controls spindle dynamics.** (A–C) HeLa cells were transfected with siRNAs and stained for pericentrin (green), β-tubulin (red), and DNA (blue). Maximum projections from deconvolved z stacks of representative control or DDA3-depleted HeLa cells are shown in A. Images were acquired under a constant exposure time for the β-tubulin channel. Pole-to-pole distances (B) were quantified by pericentrin immunofluorescence in control (n = 10) or DDA3-depleted (n = 10) metaphase cells. Total immunofluorescence intensity for β-tubulin on the metaphase spindle (n = 10 cells for each quantification) was quantified and plotted in C. In addition, siRNA-transfected cells were treated with 1 μg/ml nocodazole for 4 min at 37°C or incubated at 4°C for 35 min, and MT fluorescence intensity of metaphase cells (n = 10 cells for each quantification) was quantified and normalized to their respective siControl samples (C). *, $P < 3 \times 10^{-5}$; **, $P < 10^{-3}$ (B; two-tailed t test). *, $P < 3 \times 10^{-4}$; **, $P < 10^{-5}$; ***, $P < 4 \times 10^{-4}$ (C; two-tailed t test relative to their respective siControl cells). (D) HeLa and HeLa/GFP–DDA3 cells were not treated, treated with 1 μg/ml nocodazole for 2 min at 37°C, or incubated at 4°C for 20 min. Cells were then stained for GFP, β-tubulin, and DNA, and MT fluorescence intensity of metaphase cells (n = 10 cells for each quantification) was quantified and normalized to their respective HeLa samples. *, $P < 5 \times 10^{-3}$; **, $P < 4 \times 10^{-2}$; ***, $P < 6 \times 10^{-3}$ (two-tailed t test relative to their respective HeLa cells). (E–G) Control or DDA3-depleted HeLa cells were treated with 1 μg/ml nocodazole for 10 min at 37°C to completely depolymerize the mitotic spindle. Nocodazole-treated cells were washed twice with prewarmed PBS, released into fresh media, and fixed at 4 (E–G), 6 (F), and 10 min (F) after release. Shown in E are maximum projections from deconvolved z stacks of representative cells stained for β-tubulin (red) and DNA (blue). Images for β-tubulin were acquired under a constant exposure time. β-tubulin immunofluorescence intensity on metaphase spindles was quantified and normalized to their respective siControl sample at the 4-min time point (n = 10 cells for each quantification in F and G). *, $P < 9 \times 10^{-4}$; **, $P < 5 \times 10^{-4}$; ***, $P < 3 \times 10^{-2}$ (F; two-tailed t test relative to their respective siControl cells at the corresponding time points). *, $P < 3 \times 10^{-3}$ (G; two-tailed t test). (H) HeLa/GFP and HeLa/GFP–DDA3 cells were treated with 1 μg/ml nocodazole for 10 min at 37°C, washed with prewarmed PBS, and then released into fresh media for the indicated time. The β-tubulin immunofluorescence intensity on metaphase spindles was measured as described in F. *, $P < 0.047$; **, $P < 0.022$ (two-tailed t test relative to their respective GFP cells at the corresponding time points). (I) HeLa cells stably expressing GFP–α-tubulin were transfected with siRNAs. GFP fluorescence intensity was acquired every 0.58 s while a photobleaching laser was focused to a diffraction-limited spot in the cytoplasm away from the spindle. 10 half-spindles from 10 metaphase cells were quantified and fluorescence signals for each half-spindle were normalized to their intensity at 0 s. The 10 half-spindles were then averaged at each time point to generate mean traces. Turnover half-lives for GFP–α-tubulin on the spindle were calculated from the averaged fluorescence signal traces. The standard errors were calculated every fifth time point and are shown in the plots. P-value is from two-tailed t test. (J) Velocity of sister chromatid segregation at anaphase A was measured in control and DDA3 knockdown cells from time-lapse images shown in Fig 3 (A and B; n = 100 anaphase cells for each quantification). *, $P < 3 \times 10^{-2}$; **, $P < 3 \times 10^{-3}$ (two-tailed t test). AU, arbitrary units. Error bars show SEM. Bars, 5 μm.

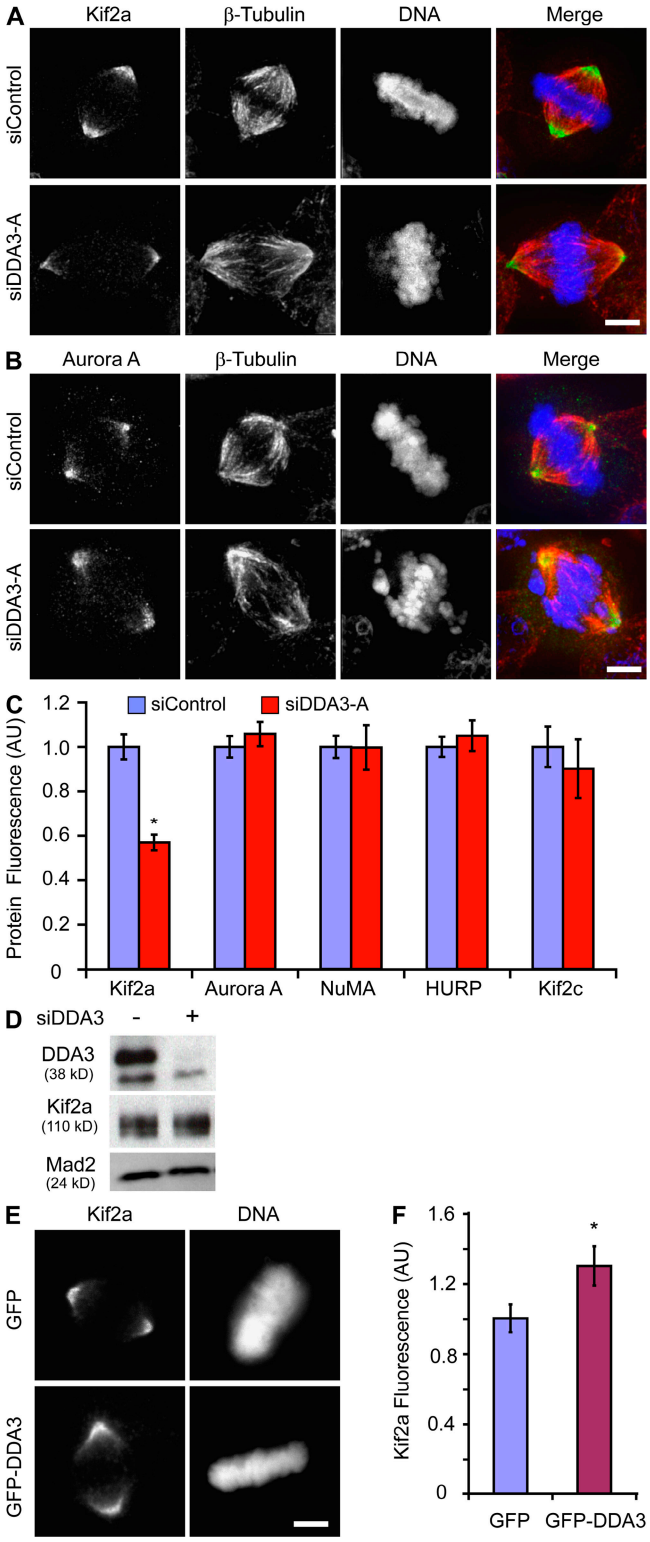

Figure 5. **DDA3 recruits Kif2a to the mitotic spindle and spindle poles.** (A–D) HeLa cells were transfected with siRNAs and stained at 62 h after transfection for various markers of the mitotic spindle and spindle poles. Shown in A and B are maximum projections from deconvolved z stacks of representative cells stained for Kif2a (A, green)/Aurora A (B, green), β-tubulin (red), and DNA (blue). Images were acquired under a constant exposure time for each channel. Immunofluorescence intensities for Kif2a, Aurora A, NuMA, HURP, and Kif2c in metaphase cells were quantified and normalized to their respective siControl samples (n = 10 cells for each quantification in C). The effect of DDA3 knockdown on the levels of the Kif2a protein was analyzed by Western blotting (D). *, $P < 10^{-5}$ (two-tailed t test). (E and F) Shown in E are maximum projections from deconvolved z stacks of representative HeLa/GFP or HeLa/GFP–DDA3 stained for Kif2a and DNA. Images were acquired under a constant exposure time in the Kif2a channel and Kif2a immunofluorescence intensity in metaphase cells was quantified and plotted (n = 10 cells in F). *, $P < 0.05$ (two-tailed t test). AU, arbitrary units. Error bars show SEM. Bars, 5 μm.

to 773 ± 121 s in siKif2a-depleted cells (Fig. 6 I), indicating that Kif2a promotes spindle turnover. Consistent with its role in spindle dynamics, knockdown of Kif2a reduced the interkinetochore distance/tension in metaphase cells as well as the rate of chromosome segregation in anaphase cells (Fig. 6, J and K), which is similar to those phenotypes found in DDA3 knockdown cells.

Similar phenotypes on spindle dynamics in DDA3- and Kif2a-depleted cells (Fig. 4 vs. Fig. 6) suggest that they act in the same pathway. In contrast to the effect of DDA3 on Kif2a localization, knockdown of Kif2a did not affect the localization of DDA3 (unpublished data), which is consistent with DDA3 acting upstream of Kif2a for its recruitment, which, in turn, regulates spindle dynamics.

DDA3 directly interacts with Kif2a in an MT-dependent manner

To determine whether DDA3 is an immediate upstream regulator of Kif2a, we explored a possible physical interaction between DDA3 and Kif2a. Myc-tagged DDA3 was cotransfected with GFP-Kif2a or GFP in 293T cells, and its association with DDA3 was analyzed by immunoprecipitation with an anti-GFP antibody. Myc-DDA3 specifically precipitated with GFP-Kif2a but not with GFP (Fig. 7 A).

Next, we determined whether the interaction between DDA3 and Kif2a is regulated in the cell cycle. As our anti-DDA3 antibody did not immunoprecipitate endogenous DDA3 and as no anti-Kif2a antibody was available for immunoprecipitation, we turned to our stable GFP–DDA3 cell line. GFP–DDA3 cells were harvested as asynchronous cells, as late G2 cells at 9 h after release from a double-thymidine arrest, or as mitotic cells after taxol treatment. GFP–DDA3 were immunoprecipitated with an anti-GFP antibody and associated Kif2a was analyzed by Western blotting. Endogenous Kif2a coimmunoprecipitated with GFP–DDA3 (Fig. 7 B). This interaction was specific, as a control protein, Mad2, did not coprecipitate with GFP–DDA3 and as nonspecific IgG precipitated neither Kif2a nor DDA3. Furthermore, coprecipitation of Kif2a was not caused by a nonspecific binding of Kif2a to the anti-GFP antibody, as demonstrated by comparing the association of Kif2a with the anti-GFP immunoprecipitates from GFP–DDA3 cells versus from parental HeLa cells (Fig. 7 C, lanes 1 and 6; and Fig. 7 D). We noticed that the amounts of the DDA3–Kif2a complex increased from asynchronous cells to G2 (Fig. 7 B, TT9) and mitotic (Fig. 7 B, Taxol) cells, correlating with the increase in the levels of the GFP–DDA3 protein, indicating a mechanism for regulation of this complex in the cell cycle.

As DDA3 was expressed as a GFP fusion protein in GFP–DDA3 cells, it is formally possible that Kif2a immunoprecipitated in Fig. 7 B because of its interaction with GFP not DDA3.

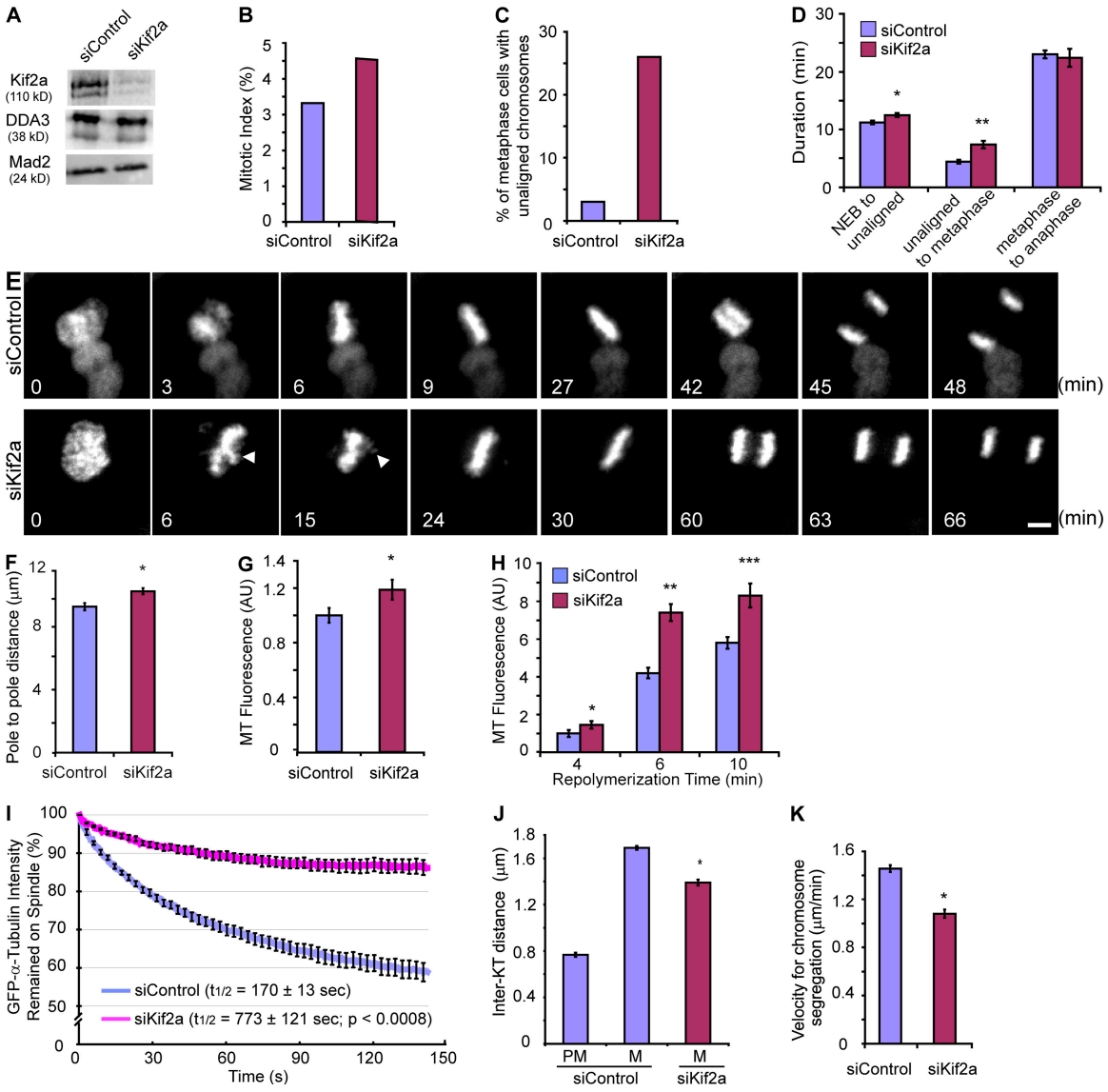

Figure 6. **Kif2a controls spindle dynamics.** (A–C, F, and G) HeLa cells were transfected with a control or a Kif2a-specific siRNA and analyzed at 62 h after transfection by Western blotting (A), FACS, or immunofluorescence staining of β-tubulin and pericentrin. Mitotic index was determined by FACS with anti-MPM2 antibody staining (B), and the percentage of metaphase cells with unaligned chromosomes over total metaphase cells (n = 100 cells; C) was quantified. Pole-to-pole distances (F) and the MT fluorescence intensity (G) in metaphase cells were quantified and plotted (n = 10 cells each). *, $P < 4 \times 10^{-3}$ (F). *, $P < 0.06$ (G; two-tailed t test). (D and E) HeLa/GFP-Histone H2B cells were transfected with siRNAs and imaged for GFP-Histone H2B by time lapse. Quantification of mitotic duration (D) in knockdown cells (n = 30 cells) was determined as described in Fig 3 A, and still frames from time-lapse images of representative cells are shown in E. Arrowheads in E point to unaligned chromosomes. *, $P < 0.016$; **, $P < 0.00012$ (two-tailed t test). (H) Control or Kif2a-depleted cells were treated with 1 μg/ml nocodazole for 15 min at 37°C, washed, released into fresh media, and stained for β-tubulin at the indicated time points after release. MT fluorescence intensity in released cells was quantified and normalized to the siControl sample at the 4-min time point (n = 10 cells). *, $P < 0.55$; **, $P < 0.03$; ***, $P < 0.11$ (two-tailed t test relative to their respective siControl cells at the corresponding time points). (I) HeLa cells stably expressing GFP–α-tubulin were transfected with siRNAs, and the half-lives of GFP–α-tubulin on the spindle were measured as described in Fig 4 I. (J) Control or Kif2a-depleted cells were stained for Hec1 and CREST and interkinetochore (Inter-KT) distance in prometaphase and metaphase cells measured from >100 kinetochore pairs in five cells for each quantification. *, $P < 9.3 \times 10^{-20}$ (two-tailed t test relative to siControl metaphase cells). (K) Velocity of sister chromatid segregation at anaphase A was measured in control and Kif2a knockdown cells from time-lapse images shown in Fig 6 (D–E; n = 40 anaphase cells for each quantification). *, $P < 2.5 \times 10^{-11}$ (two-tailed t test). AU, arbitrary units. Error bars show SEM. Bar, 10 μm.

To conclusively rule out this possibility, we took advantage of a Tev protease site engineered between the GFP and DDA3 in the fusion protein. The GFP–DDA3 complex was immunoprecipitated by the anti-GFP antibody beads (Fig. 7 C, lane 1) and then incubated with a buffer in the presence (Fig. 7 C, lanes 4 and 5) or absence (Fig. 7 C, lanes 2 and 3) of the Tev protease. The GFP–DDA3–Kif2a complex remained on the beads in the absence of the Tev protease, whereas in the presence of Tev protease the DDA3–Kif2a complex was released into supernatant, whereas the GFP protein remained on the beads, demonstrating the specificity of the DDA3–Kif2a interaction.

As both DDA3 and Kif2a are associated with the mitotic spindle, we analyzed whether their interaction requires the presence of MTs. GFP–DDA3 cells were arrested in mitosis by either

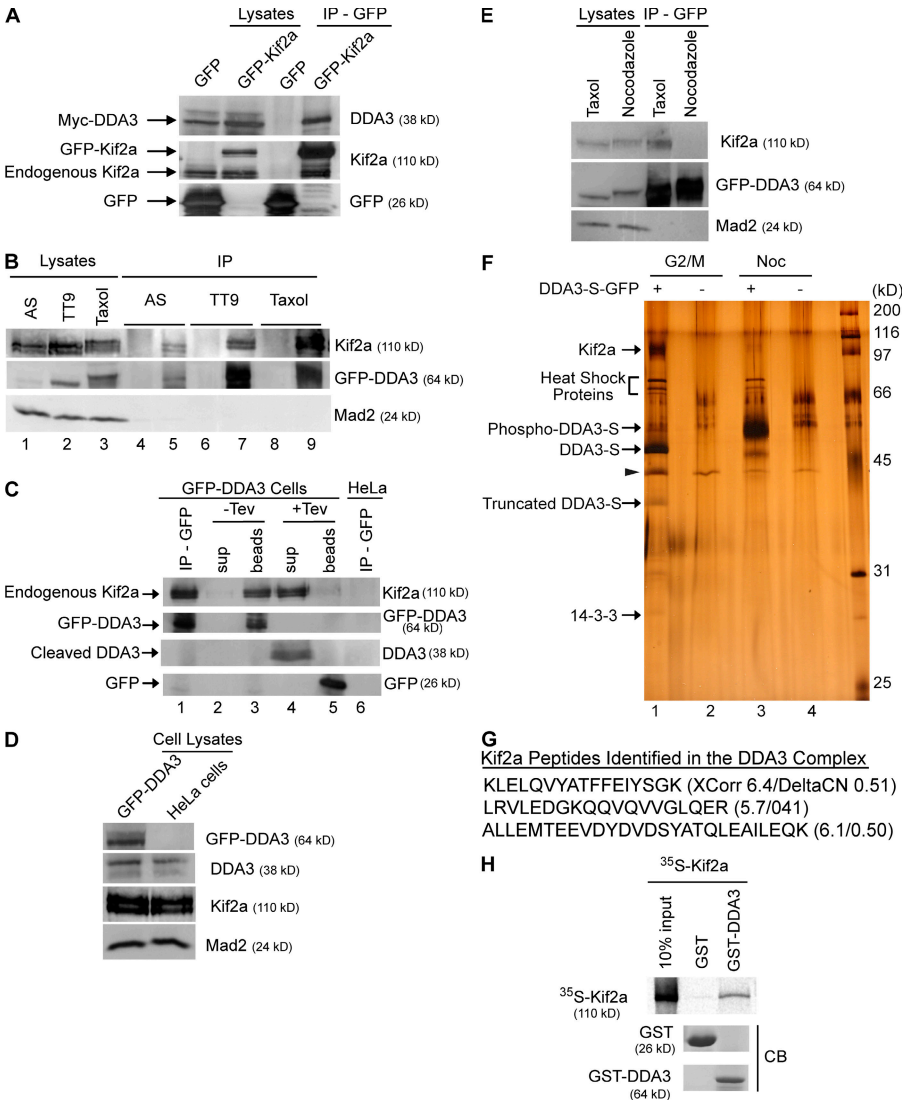

Figure 7. **DDA3 directly interacts with Kif2a.** (A) Myc-DDA3 was cotransfected with GFP-Kif2a or GFP into 293T cells. Lysates of transfected 293T cells were immunoprecipitated (IP) with anti-GFP antibodies followed by Western blotting. (B) HeLa/GFP–DDA3 cells were synchronized by a double-thymidine treatment, released, and harvested at 9 h after release (TT9). Alternatively, 1 μM Taxol was added to cells at 8 h after release from the double-thymidine arrest and then harvested at 12 h after release (Taxol sample). Cell lysates were immunoprecipitated with nonspecific IgG (lanes 4, 6, and 8) or with anti-GFP antibodies (lanes 5, 7, and 9) followed by Western blotting. AS, asynchronous cells. (C and D) HeLa/GFP–DDA3 (C, lanes 1–5) or HeLa (C, lane 6) cells were synchronized by a double-thymidine arrest, released, and harvested at 9 h after release. The levels of Kif2a and DDA3 in total cell lysates were determined by Western blotting (D). GFP–DDA3 was immunoprecipitated with anti-GFP antibody beads, incubated with or without the Tev protease, separated into supernatant (sup) and beads, and then assayed by Western blotting (C). (E) HeLa/GFP–DDA3 cells were synchronized by a thymidine arrest and release into fresh media. 1 μM taxol or 150 ng/ml nocodazole was added at 8 h after release and cells were harvested at 12 h after release. GFP–DDA3 was immunoprecipitated with anti-GFP antibodies and associated Kif2a was analyzed by Western blotting. (F and G) Cells stably expressing DDA3-S-GFP were synchronized by a single thymidine arrest and harvested at 8 h after release to enrich G2 and M cells (G2/M). Alternatively, cells were harvested after incubation with 250 ng/ml nocodazole for 18 h (Noc). The DDA3 complex was tandem affinity purified from the DDA3-S-GFP cells (F, lanes 1 and 3) or from the control parental cells (lanes 2 and 4), separated by SDS–PAGE, and visualized by silver staining. Arrowhead points to the precision protease used during purification to cleave its recognition site engineered between S and GFP tags. Peptides of Kif2a identified in the DDA3 complex are listed in G with XCorr and DeltaCN scores indicated. (H) Recombinant GST-DDA3 and GST were incubated with ^{35}S-Kif2a that had been synthesized in reticulocyte lysates in vitro. GST and GST-DDA3 were then purified by glutathione beads and associated Kif2a analyzed by SDS-PAGE. CB, Coomassie blue staining.

taxol or nocodazole, and the GFP–DDA3 complex was purified by the anti-GFP antibody beads. Kif2a was coprecipitated with DDA3 only in the presence of taxol but not nocodazole (Fig. 7 E). Thus, MTs promote the DDA3–Kif2a interaction.

To determine whether DDA3 interacts with proteins other than Kif2a to control spindle dynamics, we established a HeLa S3 cell line stably expressing DDA3 C-terminally tagged with the S-peptide and GFP. The DDA3 complex was tandem affinity purified from late G2/mitotic cells and from nocodazole-treated cells, and proteins associated with DDA3 were analyzed by mass spectrometry (Fig. 7 F). Kif2a was identified as the major DDA3-interacting protein with high confidence, as reflected in the high scores for XCorr and DeltaCN (Fig. 7, F and G). Other proteins identified were a 14-3-3 protein and heat-shock proteins. No tubulin was detected in the DDA3 complex either by mass spectrometry or Western blotting (data not shown), indicating that copurification of Kif2a with DDA3 was not mediated through MTs. In contrast, depolymerization of MTs by nocodazole abolished the interaction between DDA3 and Kif2a in mitotic cells (Fig. 7 F), suggesting a role of the mitotic spindle in the formation of the DDA3–Kif2a complex.

We next tested whether DDA3 directly interacts with Kif2a in an in vitro binding assay. ^{35}S-Kif2a was synthesized in vitro and then incubated with recombinant GST-DDA3 or GST. Kif2a specifically copurified with GST-DDA3 but not with GST (Fig. 7 H). Thus, DDA3 and Kif2a directly interact, albeit at a lower level in the absence of MTs. We concluded that DDA3 regulates MT dynamics via a direct interaction with and concurrent recruitment of Kif2a to the mitotic spindle and spindle poles.

Discussion

Through a functional genomic analysis combined with a targeted siRNA screen for mitotic regulators (Wong and Fang, 2006; Zhao et al., 2006; Seki and Fang, 2007), we identified DDA3 as

a regulator for spindle dynamics and for mitotic progression. Among DDA3-depleted metaphase cells, a high percentage had unaligned chromosomes, even though kinetochores of these chromosomes were attached to MTs (Figs. 1 and 3). For chromosomes aligned at the metaphase plate, knockdown of DDA3 substantially reduced the tension across sister kinetochores. Once DDA3 knockdown cells entered anaphase, the velocity of chromosome segregation was substantially reduced (Fig. 4). At the cellular level, DDA3 associates with the mitotic spindle and controls MT dynamics. DDA3 reduces MT polymerization kinetics and promotes MT turnover on the spindle. Molecularly, DDA3 directly interacts with the MT depolymerase Kif2a and recruits it to the mitotic spindle and spindle poles, thereby increasing the spindle MT turnover rate. Our study defines DDA3 as a novel MT-destabilizing protein that regulates the MT depolymerase Kif2a.

Mechanism of DDA3 function in spindle dynamics and mitotic progression

Dynamic turnover of the mitotic spindle is essential for congression of chromosomes at prometaphase, establishment of tension at metaphase, and segregation of sister chromatids at anaphase (Kline-Smith and Walczak, 2004). In fact, depolymerization at MT ends creates forces sufficient for chromosome movement (Koshland et al., 1988; Grishchuk and McIntosh, 2006). MT depolymerization on the mitotic spindle is controlled by MT depolymerases, such as Kif2a, Kif2b, Kif2c/MCAK, and Kif18, with Kif2a and b acting at minus ends and Kif2c/MCAK and Kif18a at plus ends (Ganem and Compton, 2004; Kline-Smith and Walczak, 2004; Wordeman, 2005; Mayr et al., 2007). The concerted action of these depolymerases controls bipolar spindle assembly, kinetochore capture, and chromosome movement in mitosis.

We showed that DDA3 regulates spindle dynamics but not spindle assembly. Depletion of DDA3 increased the steady-state levels of MTs and reduced the turnover rate of the mitotic spindle (Fig. 4), indicating a role for DDA3 in destabilizing MTs in mitosis. Knockdown of DDA3 did not affect the capture of kinetochores by MTs (Fig. 3). In fact, the MT attachment to kinetochores was more efficient in prometaphase cells depleted of DDA3, as indicated by lower kinetochore Mad2 signals in these cells compared with control prometaphase cells (Fig. 2). This likely results from an increase in spindle MT mass in knockdown cells. As dynamic turnover at plus ends of spindle MTs contributes to efficient capture of kinetochores (Kline-Smith and Walczak, 2004), depletion of DDA3 is unlikely to affect the MT dynamics at plus ends. In contrast, depletion of DDA3 generated a high frequency of unaligned chromosomes with attached MTs and abolished interkinetochore tension for aligned chromosomes, suggesting that the MT dynamics, most likely at minus ends, is altered in DDA3 knockdown cells.

DDA3 is a novel protein with no known sequence motifs. Although recombinant DDA3 has MT binding and bundling activities, it has no depolymerase activity in vitro (Hsieh et al., 2007; unpublished data). We showed here that DDA3 specifically interacts with the minus-end depolymerase Kif2a but not with other depolymerases, such as Kif2b, Kif2c, and Kif18. Importantly, knockdown of DDA3 and Kif2a generated similar phenotypes on MT levels and spindle dynamics (Figs. 4 and 6), suggesting that DDA3 and Kif2a act in the same pathway. Depletion of DDA3 reduced the levels of Kif2a on the spindle and spindle poles, but not vice versa (Fig. 5), suggesting that DDA3 is likely to act upstream of Kif2a to recruit it to the mitotic spindle and spindle poles.

Although DDA3 and Kif2a form a complex to regulate MT mass and spindle dynamics in mitosis, each protein is likely to have mitotic functions independent of the complex. For example, Kif2a is required for the bipolarity of the mitotic spindle, as complete depletion of Kif2a results in a monopolar spindle (Ganem and Compton, 2004; Ganem et al., 2005). In addition, knockdown of DDA3 and Kif2a do not reduce MT turnover to the same degree (Figs. 4 and 6). DDA3 also has mitotic functions independent of Kif2a, as knockdown of DDA3 generated a higher frequency of unaligned chromosomes in metaphase cells, a longer delay at metaphase, and larger reductions in metaphase interkinetochore tension and anaphase chromosome segregation velocity than knockdown of Kif2a (Figs. 1, 3, 4, and 6). Thus, it is likely that Kif2a only partially contributes to DDA3 function in mitosis and that DDA3 regulates additional molecular targets to control chromosome alignment and segregation. It is interesting to note that a recent study reports an association of DDA3 with the MT plus-end tracking protein EB3 based on a yeast two-hybrid assay (Hsieh et al., 2007). Although we failed to detect a stable DDA3-EB3 interaction during mitosis (unpublished data), it remains to be determined whether DDA3 and EB3 act in a same mitotic pathway and whether DDA3 regulates the function of EB3 to control chromosome congression and segregation.

Mechanism for targeting Kif2a to MT minus ends at spindle poles

DDA3 promotes the localization of Kif2a to spindle poles. Although formation of the DDA3–Kif2a complex requires the presence of MTs, the interaction between DDA3 and Kif2a is direct and not mediated through MTs (Fig. 7). It is likely that association of DDA3 and Kif2a with MTs triggers conformational changes in either or both proteins that increase their binding affinity to each other. In contrast, localization of DDA3 and Kif2a only partially overlaps on the mitotic spindle. Although Kif2a is concentrated around spindle pole regions, DDA3 spans the entire mitotic spindle without obvious enrichment at spindle poles. Thus, DDA3 and Kif2a form a dynamic complex on the mitotic spindle. Even though recombinant Kif2a can bind to MT ends in the absence of ATP (Noda et al., 1995; Desai et al., 1999), it is likely that through the complex formation, DDA3 increases the affinity of Kif2a to the entire MT. Once loaded onto the mitotic spindle assisted by DDA3, Kif2a then dissociates from the complex and is transported toward the minus ends of MTs to increase spindle dynamics and MT flux. In this model, DDA3 reduces the complexity of targeting Kif2a to spindle poles from a three-dimensional search for MT minus ends to a two-dimensional search for DDA3 along the entire MT polymers, thereby greatly increasing the loading efficiency of Kif2a to spindle poles. In a mutually nonexclusive model, the DDA3–Kif2a complex formed on the mitotic spindle may dissociate

from spindle MTs to control cytoplasmic MT polymerization and depolymerization in mitosis. It remains to be determined whether DDA3 in the Kif2a complex alters the MT depolymerase activity of Kif2a.

Proper MT dynamics is also essential to cell and tissue morphogenesis outside the cell cycle. For example, Kif2a is highly expressed in neurons, in which Kif2a depolymerizes MTs at the growth cone edge to suppress the growth of axonal collateral branches (Homma et al., 2003). As DDA3 is also enriched in the brain (Lo et al., 1999), it is likely that DDA3 may also regulate Kif2a function in differentiated cells during development. Elucidation of the physiological function and the biochemical mechanism for this unique MT-destabilizing protein DDA3 in the cell cycle will open the door to investigate its function and regulation in cell and tissue morphogenesis in general.

Materials and methods

Plasmids and antibodies

The full-length DDA3 gene was subcloned into the pET28a vector (Invitrogen) with an N-terminal His tag and into the pGEX vector (GE Healthcare) with an N-terminal GST tag, expressed in *Escherichia coli*, and purified. GFP–DDA3, Myc-DDA3, and GFP-Kif2a were subcloned into pCS2+ with an N-terminal GFP or Myc tag.

Recombinant His-DDA3 was used to immunize rabbits for production of antiserum. Anti-DDA3 antibodies were subsequently purified against the antigen. The anti-GFP sera were raised against the full-length recombinant GFP and affinity purified. The anti-Kif2c antibody was provided by C.E. Walkzak (Indiana University, Bloomington, IN), anti-pericentrin was provided by T. Stearns (Stanford University, Palo Alto, CA), and anti-NuMA was provided by D. Compton (Dartmouth Medical School, Hanover, NH). Rabbit antibodies against Mad2, BubR1, and HURP were described previously (Wong and Fang, 2006). Anti–β-tubulin E7 mAb was obtained from the Developmental Studies Hybridoma Bank. The following antibodies were obtained from commercial sources: CREST (Antibodies Incorporated); anti-Hec1 (GeneTex, Inc.); anti-Kif2a (Novus Biologicals); and anti–cyclin B1, anti–Aurora A, anti-Hsp70, anti-myc, and anti-p38MAPK antibodies (Santa Cruz Biotechnology, Inc.).

Cell culture, siRNAs, and transfection

HeLa S3, HeLa, and 293T cells were cultured in DME containing 10% FBS (Invitrogen) and antibiotics. Cells were synchronized at the G1/S boundary by a double-thymidine treatment or at prometaphase by a thymidine-nocodazole treatment, as previously described (Fang et al., 1998a,b).

siRNAs were synthesized by Thermo Fisher Scientific. The sequences targeting DDA3 were 5′-AAGCAAGACTTCAGTAGCATT-3′ and 5′-CCACCGAAGTGACCCAAATTT-3′. The sequence targeting Kif2a was 5′-GGAATGGCATCCTGTGAAA-3′. The control siRNA was 5′-CGTACGCGGAATACTTCGATT-3′. siRNAs were transfected into HeLa cells using DharmaFect 1 (Thermo Fisher Scientific).

DNA transfection was performed using Effectene (QIAGEN) or Lipofectamine 2000 (Invitrogen). Cells cotransfected with GFP-Kif2a and Myc-DDA3 were analyzed at 36 h after transfection by immunoprecipitation and Western blotting.

Immunoprecipitation, immunofluoresence, and live cell imaging

Rabbit antibodies against GFP were coupled to Affi-Prep Protein A beads (Bio-Rad Laboratories) at a concentration of 0.3 mg/ml. HeLa or HeLa S3 cells were lyzed in the NP-40 lysis buffer (50 mM Hepes, pH 7.4, 200 mM KCl, 0.3% NP-40, 10% glycerol, 1 mM EGTA, 1 mM $MgCl_2$, 0.5 mM DTT, 0.5 μM microcystin, and 10 μg/ml each of leupeptin, pepstatin, and chymostatin). Lysates were centrifugated, incubated with protein A beads coupled with preimmune rabbit IgG at 4°C for 1 h, and then incubated with protein A beads coupled with anti-GFP antibodies at 4°C overnight. Antibody beads were recovered by centrifugation, washed five times with the lysis buffer in the presence of 500 mM KCl and then twice with the lysis buffer, analyzed by SDS-PAGE, and immunoblotted with appropriate antibodies.

HeLa cells on cover glasses were fixed with −20°C methanol for 5 min. Alternatively, cells were extracted with the PHEMT buffer (60 mM Pipes, 25 mM Hepes, pH 6.9, 10 mM EGTA, 4 mM $MgCl_2$, and 0.5% Triton X-100; Fig. 3, D–F) or the BRB80-T buffer (80 mM Pipes, pH 6.8, 1 mM $MgCl_2$, 5 mM EGTA, and 0.5% Triton X-100; Fig. 2, A–C) and then fixed with 4% PFA for 15 min at room temperature. Subsequently, cells were permeabilized and blocked with PBS-BT (PBS, 3% BSA, and 0.1% Triton X-100) for 30 min at room temperature. Coverslips were subsequently incubated in primary and Alexa Fluor 594– and 488–coupled secondary antibodies diluted in PBS-BT. Images were acquired with Openlab 5.2 software (Improvision) under a microscope (Axiovert 200M; Carl Zeiss, Inc.) using a 1.4 NA plan-Apo 100× oil immersion lens and a charge-coupled device camera (Orca-ER; Hamamatsu). Deconvolved images were obtained using AutoDeblur v9.1 and AutoVisualizer v9.1 (Media Cybernetics, Inc.).

For time-lapse microscopy, HeLa cells stably expressing GFP-H2B were cultured in Leibovitz's L-15 medium (Invitrogen) supplemented with 10% FBS (Invitrogen) and 2 mM L-glutamine (Invitrogen). Cells were placed into a sealed growth chamber heated to 37°C and observed on a microscope (Axiovert 200M) with a 0.4 NA Achro-plan 20× lens. Images were acquired every 3 min for 5 h with Openlab 5.2 software. For confocal time-lapse microscopy, HeLa cells stably expressing GFP-CenpA were observed using a 1.4 NA Plan-Apo 63× oil immersion objective with an UltraView confocal scanner unit (PerkinElmer) and images were acquired every 6 s.

For FLIP, HeLa cells stably expressing GFP–α-tubulin (a gift from L. Wordeman, University of Washington, Seattle, WA) were transfected with a control or siDDA3-1 and placed in a sealed growth chamber heated to 37°C. Cytoplasmic GFP–α-tubulin was photobleached with a fiber-optically pumped dye laser and images were acquired at 0.58-s intervals for 140 s with SlideBook 4.0 (Intelligent Imaging Innovations, Inc.) under a microscope (Axiovert 200M) with a 1.4 NA 100× oil immersion objective and a CoolSnap HQ charge-coupled device camera (Photometrics). 10 half-spindles from 10 metaphase cells in each transfection were analyzed by measuring the absolute GFP–α-tubulin fluorescence intensity in a defined circular area contained entirely within each half-spindle. Fluorescence intensities were not background corrected because of the minimal contribution to fluorescence signal from cytoplasmic GFP–α-tubulin within the spindle. Fluorescence intensities for each half-spindle were normalized to their maximum intensity at the beginning of the time lapse and the 10 normalized datasets were averaged to generate a single trace for each transfection. Half-lives for GFP–α-tubulin on the spindle were calculated by linear regression of the averaged traces.

DDA3 proteomics

Tandem purification of the DDA3 complex. The DDA3 gene was fused to GFP and S-peptide tags in the pBabe-Puro vector and subsequently transfected into Phoenix-Ampho packaging cells. The viral supernatant was used to infect HeLa S3 cells to isolate stable clones after selection with 0.4 μg/ml puromycin for 2 wk. A clone stably expressing DDA3-S-GFP gene at a level comparable to that of endogenous DDA3 was used to purify the DDA3 complex as described previously (Cheeseman et al., 2004).

Liquid chromatography–tandem mass spectrometry. A 100-μm i.d. capillary with a 5-μm pulled tip was packed with 10 cm of 5-μm Aqua C18 material (Phenomenex). The desalting column was then equilibrated for 30 min with Buffer A (5% acetonitrile/0.1% formic acid) and the protein digest was pressure loaded onto it. The column was placed inline with a quaternary HPLC (1100; Agilent Technologies) and analyzed by a one-step separation that consisted of a 120-min gradient from 0 to 100% Buffer B (80% acetonitrile/0.1% formic acid). As peptides eluted from the microcapillary column, they were electrosprayed directly onto an LTQ mass spectrometer (Thermo Fisher Scientific) with the application of a distal 2.4-kV spray voltage. A cycle of one full-scan mass spectrum (400–1,400 m/z) was followed by three data-dependent tandem mass spectrometry spectra at a 35% normalized collision energy.

Analysis of tandem mass spectrometry. Tandem mass spectrometry spectra were analyzed by using the following software analysis protocol. Poor-quality spectra were removed from the dataset by using an automated spectral quality assessment algorithm (Bern et al., 2004). Tandem mass spectrometry spectra remaining after filtering were searched with the SEQUEST algorithm (Eng et al., 1994) against a human database concatenated to a decoy database in which the sequence for each entry in the original database was reversed (Peng et al., 2003). No enzyme specificity was considered for any search. SEQUEST results were assembled and filtered by using the DTASelect program (version 2.0; Tabb et al., 2002). DTASelect 2.0 uses a linear discriminant analysis to dynamically set XCorr and DeltaCN thresholds for the entire dataset to achieve a user-specified

false-positive rate (5% in this analysis). The false-positive rates are estimated by the program from the number and quality of spectral matches to the decoy database.

We thank Drs. Claire E. Walkzak, Duane Compton and Tim Stearns for antibodies and Linda Wordeman for GFP–α-tubulin cell line. We are grateful to Dr. James Nelson (Stanford University) for help with FLIP experiments and to members of the Fang laboratory for discussions.

This work was supported by a postdoctoral fellowship from the Korea Research Foundation of the Korean Government (MOEHRD; KRF-2006-352-C00057 to C.-Y. Jang), by a Burroughs-Wellcome Career Award in Biomedical Research (G. Fang), and by grants from National Institutes of Health (GM062852 to G. Fang and HL079442 and RR11823-10 to J.R. Yates).

Submitted: 7 November 2007
Accepted: 19 March 2008

References

Bern, M., D. Goldberg, W.H. McDonald, and J.R. Yates III. 2004. Automatic quality assessment of peptide tandem mass spectra. *Bioinformatics.* 20:i49–i54.

Cheeseman, I.M., S. Niessen, S. Anderson, F. Hyndman, J.R. Yates III, K. Oegema, and A. Desai. 2004. A conserved protein network controls assembly of the outer kinetochore and its ability to sustain tension. *Genes Dev.* 18:2255–2268.

Desai, A., and T.J. Mitchison. 1997. Microtubule polymerization dynamics. *Annu. Rev. Cell Dev. Biol.* 13:83–117.

Desai, A., S. Verma, T.J. Mitchison, and C.E. Walczak. 1999. Kin I kinesins are microtubule-destabilizing enzymes. *Cell.* 96:69–78.

Eng, J.K., A.L. McCormack, and J.R. Yates. 1994. An approach to correlate tandem mass spectral data of peptides with amino acid sequences in a protein database. *J. Am. Soc. Mass Spectrom.* 5:976–989.

Fang, G., H. Yu, and M.W. Kirschner. 1998a. The checkpoint protein MAD2 and the mitotic regulator CDC20 form a ternary complex with the anaphase-promoting complex to control anaphase initiation. *Genes Dev.* 12:1871–1883.

Fang, G., H. Yu, and M.W. Kirschner. 1998b. Direct binding of CDC20 protein family members activates the anaphase-promoting complex in mitosis and G1. *Mol. Cell.* 2:163–171.

Gadde, S., and R. Heald. 2004. Mechanisms and molecules of the mitotic spindle. *Curr. Biol.* 14:R797–R805.

Ganem, N.J., and D.A. Compton. 2004. The KinI kinesin Kif2a is required for bipolar spindle assembly through a functional relationship with MCAK. *J. Cell Biol.* 166:473–478.

Ganem, N.J., K. Upton, and D.A. Compton. 2005. Efficient mitosis in human cells lacking poleward microtubule flux. *Curr. Biol.* 15:1827–1832.

Grishchuk, E.L., and J.R. McIntosh. 2006. Microtubule depolymerization can drive poleward chromosome motion in fission yeast. *EMBO J.* 25:4888–4896.

Homma, N., Y. Takei, Y. Tanaka, T. Nakata, S. Terada, M. Kikkawa, Y. Noda, and N. Hirokawa. 2003. Kinesin superfamily protein 2A (KIF2A) functions in suppression of collateral branch extension. *Cell.* 114:229–239.

Hsieh, P.C., J.C. Chang, W.T. Sun, S.C. Hsieh, M.C. Wang, and F.F. Wang. 2007. p53 downstream target DDA3 is a novel microtubule-associated protein that interacts with end-binding protein EB3 and activates beta-catenin pathway. *Oncogene.* 26:4928–4940.

Kline-Smith, S.L., and C.E. Walczak. 2004. Mitotic spindle assembly and chromosome segregation: refocusing on microtubule dynamics. *Mol. Cell.* 15:317–327.

Koshland, D.E., T.J. Mitchison, and M.W. Kirschner. 1988. Polewards chromosome movement driven by microtubule depolymerization in vitro. *Nature.* 331:499–504.

Lo, P.K., J.Y. Chen, W.C. Lo, B.F. Chen, J.P. Hsin, P.P. Tang, and F.F. Wang. 1999. Identification of a novel mouse p53 target gene DDA3. *Oncogene.* 18:7765–7774.

Maiato, H., J. DeLuca, E.D. Salmon, and W.C. Earnshaw. 2004. The dynamic kinetochore-microtubule interface. *J. Cell Sci.* 117:5461–5477.

Manning, A.L., N.J. Ganem, S.F. Bakhoum, M. Wagenbach, L. Wordeman, and D.A. Compton. 2007. The kinesin-13 proteins Kif2a, Kif2b, and Kif2c/MCAK have distinct roles during mitosis in human cells. *Mol. Biol. Cell.* 18:2970–2979.

Mayr, M.I., S. Hummer, J. Bormann, T. Gruner, S. Adio, G. Woehlke, and T.U. Mayer. 2007. The human kinesin Kif18A is a motile microtubule depolymerase essential for chromosome congression. *Curr. Biol.* 17:488–498.

Musacchio, A., and K.G. Hardwick. 2002. The spindle checkpoint: structural insights into dynamic signalling. *Nat. Rev. Mol. Cell Biol.* 3:731–741.

Musacchio, A., and E.D. Salmon. 2007. The spindle-assembly checkpoint in space and time. *Nat. Rev. Mol. Cell Biol.* 8:379–393.

Noda, Y., R. Sato-Yoshitake, S. Kondo, M. Nangaku, and N. Hirokawa. 1995. KIF2 is a new microtubule-based anterograde motor that transports membranous organelles distinct from those carried by kinesin heavy chain or KIF3A/B. *J. Cell Biol.* 129:157–167.

Peng, J., J.E. Elias, C.C. Thoreen, L.J. Licklider, and S.P. Gygi. 2003. Evaluation of multidimensional chromatography coupled with tandem mass spectrometry (LC/LC-MS/MS) for large-scale protein analysis: the yeast proteome. *J. Proteome Res.* 2:43–50.

Segal, E., N. Friedman, D. Koller, and A. Regev. 2004. A module map showing conditional activity of expression modules in cancer. *Nat. Genet.* 36:1090–1098.

Seki, A., and G. Fang. 2007. CKAP2 is a spindle-associated protein degraded by APC/C-Cdh1 during mitotic exit. *J. Biol. Chem.* 282:15103–15113.

Skoufias, D.A., P.R. Andreassen, F.B. Lacroix, L. Wilson, and R.L. Margolis. 2001. Mammalian mad2 and bub1/bubR1 recognize distinct spindle-attachment and kinetochore-tension checkpoints. *Proc. Natl. Acad. Sci. USA.* 98:4492–4497.

Tabb, D.L., W.H. McDonald, and J.R. Yates III. 2002. DTASelect and Contrast: tools for assembling and comparing protein identifications from shotgun proteomics. *J. Proteome Res.* 1:21–26.

Whitfield, M.L., G. Sherlock, A.J. Saldanha, J.I. Murray, C.A. Ball, K.E. Alexander, J.C. Matese, C.M. Perou, M.M. Hurt, P.O. Brown, and D. Botstein. 2002. Identification of genes periodically expressed in the human cell cycle and their expression in tumors. *Mol. Biol. Cell.* 13:1977–2000.

Wong, J., and G. Fang. 2006. HURP controls spindle dynamics to promote proper interkinetochore tension and efficient kinetochore capture. *J. Cell Biol.* 173:879–891.

Wordeman, L. 2005. Microtubule-depolymerizing kinesins. *Curr. Opin. Cell Biol.* 17:82–88.

Zhao, W.M., A. Seki, and G. Fang. 2006. Cep55, a microtubule-bundling protein, associates with centralspindlin to control the midbody integrity and cell abscission during cytokinesis. *Mol. Biol. Cell.* 17:3881–3896.